

RESEARCH ARTICLE

Structural characterization of the near-surface region of soda–lime–silica glass by X-ray photoelectron spectroscopy

Barsheek Roy¹  | Felix Baier² | Andreas Rosin¹  | Thorsten Gerdes¹ |
Stefan Schafföner³ 

¹Keylab Glass Technology, University of Bayreuth, Bayreuth, Germany

²Experimental Physics XI, University of Bayreuth, Bayreuth, Germany

³Ceramic Materials Engineering, University of Bayreuth, Bayreuth, Germany

Correspondence

Barsheek Roy, Keylab Glass Technology, University of Bayreuth, Prof.-Rüdiger-Bormann-Str. 1, 95447 Bayreuth, Germany.
Email: barsheek.roy@uni-bayreuth.de

Abstract

The structural chemistry of the near-surface region of soda–lime–silica (SLS) glass is described in terms of silicate network connectivity using X-ray photoelectron spectroscopy (XPS). A thorough investigation of O1s and Si2p spectral lines by sequential XPS measurements, accompanied by Ar⁺ sputtering, revealed the variation of concentration of bridging oxygen, non-bridging oxygen (NBO), and hydrous species (SiOH/H₂O) as a function of depth from the glass surface. The O_{total}/Si atomic ratio was calculated to vary in the range of 2.90–3.74 throughout the depth of sputtering for a total duration of 110 min, while considering each of the aforementioned oxygen speciations in the curve-fitted spectra of O1s orbital. The glass surface up to a depth of 1–3 nm had the highest O_{total}/Si ratio of 3.74, which was representative for a mechanically weak structure with Q⁰ and Q¹ species, marked by the respective linkages of four and three NBOs per silica tetrahedral unit. This dictates the vital contribution of the hydrous species associated with silanol groups to the near-surface structure of SLS glass.

KEYWORDS

glass, nanostructures, soda–lime–silica, surface, X-ray photoelectron spectroscopy

1 | INTRODUCTION

The inevitable interaction of silicate glass surface with the ambient atmosphere has been a subject of considerable research in the past.^{1–3} The detrimental effects of the consequent corrosion mechanisms are well known with respect to surface degradation phenomena associated with the availability of a micro-channelized pathway for diffusion processes through the injured, porous layer of outer glass skin.⁴

The surface structure of soda–lime–silica (SLS) glass is known to be characterized by different techniques^{5–11}; among which, X-ray photoelectron spectroscopy (XPS) is

widely used for the convenient characterization of bridging oxygens (BOs) and non-bridging oxygens (NBOs) on the topmost surface.^{7–11} However, to the best of our knowledge, there is no elaborate report on the variation of individual oxygen speciations as a function of depth from the glass surface; the scientific knowledge of which is of utmost necessity to understand the essence of surface structural chemistry, which governs the mechanical properties of the glass surface.

In this study, we endeavored to gain a thorough insight of the structural network from the surface to the bulk (up to about 100 nm) of SLS glass by XPS. XPS, when combined with ionic sputtering, is a powerful means of exploration

This is an open access article under the terms of the [Creative Commons Attribution](https://creativecommons.org/licenses/by/4.0/) License, which permits use, distribution and reproduction in any medium, provided the original work is properly cited.

© 2022 The Authors. *International Journal of Applied Glass Science* published by American Ceramics Society and Wiley Periodicals LLC.

of the depth of the glass network.^{12,13} Although previous studies reported certain drawbacks associated with argon ion (Ar^+) sputtering on SLS glass surface with relevance to change in the concentration of mobile ions (Na^+ and Ca^{2+}), while recommending a possible replacement by means of C_{60} sputtering instead.^{14–16} However, with precise technical control of the phenomenon, it is possible to minimize the effect of surface damage caused by Ar^+ sputtering and, hence, is still a widely used technique in structural glass science.

This paper is predominantly centered on exploring the variation of the structural chemistry of the near-surface region of SLS glass—reflected by the variation of concentration of BOs, NBOs, and hydrous species ($\text{SiOH}/\text{H}_2\text{O}$), which is fundamentally thought to determine the structural orientation of the silicate network governing the mechanical integrity of the surface structure. The investigations were specifically constrained to O1s and Si2p spectral lines, bearing in mind the possible influential alteration of Na1s caused by a migration of mobile ions due to Ar ion implantation.

2 | INSTRUMENTAL AND ANALYTICAL ASPECTS OF X-RAY PHOTOELECTRON SPECTROSCOPIC AND ATOMIC FORCE MICROSCOPIC MEASUREMENTS

A PHI 5000 VersaProbe III spectrometer with an Al K alpha source (1486.6 eV) was used to conduct XPS studies. Monochromatized X-rays were obtained by quartz crystal. Sequential XPS measurements were performed at specific time intervals in conjunction with Ar^+ sputtering at 5 kV. The target current on the specimen holder was 3 μA , whereas the focus beam current was 302 nA at the Faraday cup. Surface charge neutralization was achieved by the virtue of a dual-beam charge neutralization system that utilizes both a cold cathode detector hood source and a very low energy ion source (<10 eV) to provide turnkey charge neutralization. The pass energy was 26 eV, whereas the spectral resolution was about .2 eV.

As-received commercial green SLS glass in the form of square glass bottles was prepared by gently drilling (wet-cutting) cylindrical specimen from flat broad sides with a diameter of 25 mm and a thickness of 3 mm, while ensuring the absence of any mechanical injury to the surface skin of interest, which was the center of the specimen where the XPS measurements were performed. The container glass without any hot- and/or cold-end coating was used in this study. The outer surface of the container glass was subjected to XPS investigations. The obtained cylindrical specimen was immersed in a static acetone bath for 15 min to remove most organic impurities from the

surface. The surface was gently blow-dried by nitrogen gas (producer: “Riessner Gase,” purity: 99.999%, humidity $\leq 5\%$, oxygen $\leq 3\%$, hydrocarbons $\leq 2\%$) at room temperature before introducing it to the ultrahigh vacuum XPS chamber at a pressure on the order of 10^{-9} mbar. The glass surface was not polished before XPS investigations to retain the structural integrity of the as-melted state. The elemental composition of the as-received SLS glass obtained by ICP-OES analysis consisted of (in wt%) the following: 31.40% Si, 8.70% Na, 7.36% Ca, 1.14% Mg, .95% Al, .63% K, .26% Fe, and .03% Ti (rest mainly assigned to oxygen), which would correspond to the following oxide composition (in wt%): 71.4% SiO_2 , 12.4% Na_2O , 10.9% CaO, 2.0% MgO, 1.9% Al_2O_3 , .8% K_2O , .4% Fe_2O_3 , and .1% TiO_2 .

All spectral fittings were performed by MultiPak software using Gaussian–Lorentzian composite function after Shirley background correction.¹⁷ The best curve-fits in terms of lowest chi-squared values (χ^2) representative of goodness of fit are reported here. Overall, 10%-Lorentzian component was included in O1s curve-fits to take into account the uncertainty principle associated with the core hole lifetime.¹⁸ The curve-fittings were performed in an unconstrained manner¹⁰ while ensuring that the full-width at half maxima (FWHM) of overlapping peaks lie within a narrow range of less than .3 eV.

According to theory, O1s and Na1s spectral lines consist of a singlet, whereas the Si2p spectrum is typically constituted of a spin orbit doublet. The Si2p_{1/2} peak intensity was precisely assigned half the intensity of Si2p_{3/2} in accordance with theoretical requirement.¹⁹ Identical FWHM values were assigned to both peaks. The difference in binding energies (BEs) between Si2p_{1/2} and Si2p_{3/2} peaks is .617 eV. Instead of the general tradition of C1s,²⁰ the Ca2p spectral line was used as the standard reference, whereas all other peaks were auto-shifted to its reference. The technical reason behind this is the relative immobility of Ca^{2+} ions within the glass structure compared to Na^+ ions at room temperature, which apparently eliminates the necessity of its analysis, as well as the negligible presence of carbon in the studied SLS glass specimen.

The atomic force microscopy of the top surface was performed by “Bruker Dimension icon” with a z-resolution of about .1 nm. A silicon nitride cantilever tip (Bruker OTESPA-R3), with a nominal tip radius of 7 nm and a maximum tip radius of 10 nm, was used to scan in tapping mode with a set-point amplitude of 854 mV. A defined area of $1 \times 1 \mu\text{m}^2$ with 512 pixels was scanned on the top surface on three different spots. A flood mask of .2 nm was applied in the software “NanoScope Analysis” after third-order flattening, to map the surface silicate network disseminated by inherent intertetrahedral voids. The flood-masking facilitated by the software isolated the silicate islands on the

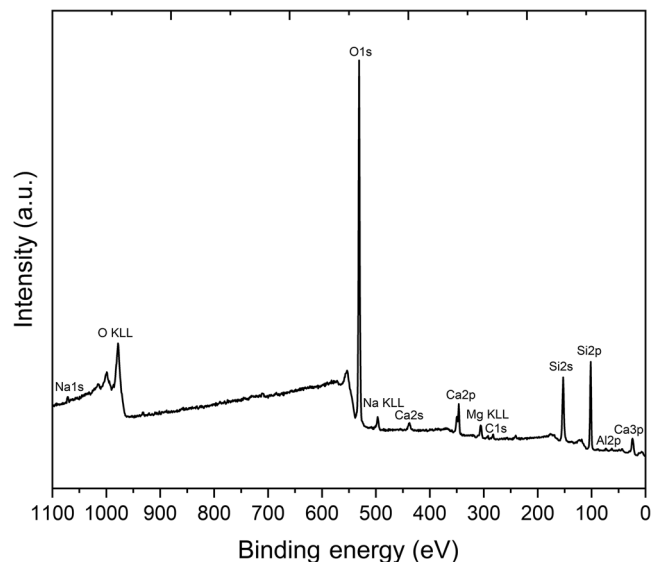


FIGURE 1 Representative survey spectrum of the top surface of soda-lime-silica (SLS) specimen

top surface to make it possible for mapping the voids with depths on the order of 500 pm.

The XPS investigations of the near-surface region of a different category of SLS glass (microscopic slides) were performed additionally, to confirm the reliability of the experimental findings on container glass surface illustrated in the paper. It is reported in the Supporting Information section.

3 | RESULTS AND DISCUSSION

The XPS survey spectrum of the top surface of SLS glass considered in this work is shown in Figure 1. The survey scan was performed up to a BE of 1100 eV, with a spectral resolution of about .2 eV.

The atomic concentrations of O1s, Si2p, Na1s, and Ca2p are shown as a function of Ar⁺ sputtering time in Figure 2. The mean composition of the near-surface region of the SLS glass considered in this study was calculated from the distribution corresponding to Figure 2 and reported in Table 1, along with the respective elemental standard deviations. Other oxides like K₂O, MgO, Al₂O₃, or Fe₂O₃ were not included as their concentrations in the glass were less than 2 wt%.

The O1s and Si2p orbitals were thoroughly studied as a function of Ar⁺ sputtering time at specific intervals, to investigate the subsurface silicate network connectivity. The local atomic bonding states of oxygen atoms on the glass surface were studied by curve-fitting of high-resolution XPS O1s spectral lines to separately determine the areal contribution of each overlapping peak.

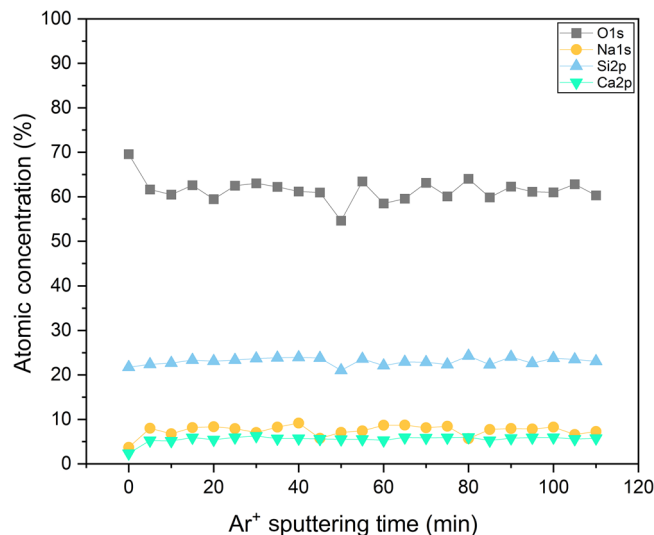


FIGURE 2 Atomic concentrations of O1s, Si2p, Na1s, and Ca2p of the near-surface region as a function of Ar⁺ sputtering time

TABLE 1 Composition of the near-surface region of the studied soda-lime-silica (SLS) glass

Element	Mean concentration (at%)	Standard deviation (at%)
O1s	61.60	2.51
Si2p	23.01	.84
Na1s	7.56	1.25
Ca2p	5.48	.68

3.1 | O1s curve-fittings

The O1s peak broadly lies within the BE range of 528–534 eV, centered around 531 eV (see Figure 3). The spectral fit is constituted of three relevant signals from the silicate structure of the glass network^{8,9,21}:

1. NBO: Si–O–Na bonding corresponding to the shoulder around 530 eV.
2. BO: Si–O–Si bonding corresponding to the central peak around 531 eV.
3. SiOH/H₂O species: Shoulder peak corresponding to higher BE around 532 eV.

The assignment of the overlapping O1s peaks to the aforementioned signals corresponding to different BEs can easily be explained by the electrostatic interactions.²¹ This is dictated by the Linus Pauling scale of electronegativity, which bears the following order of decreasing trend: H>Si>Na. Hydrogen, possessing the highest electronegativity among the three elements, has a higher tendency to attract the electron cloud of the oxygen atom. On average,

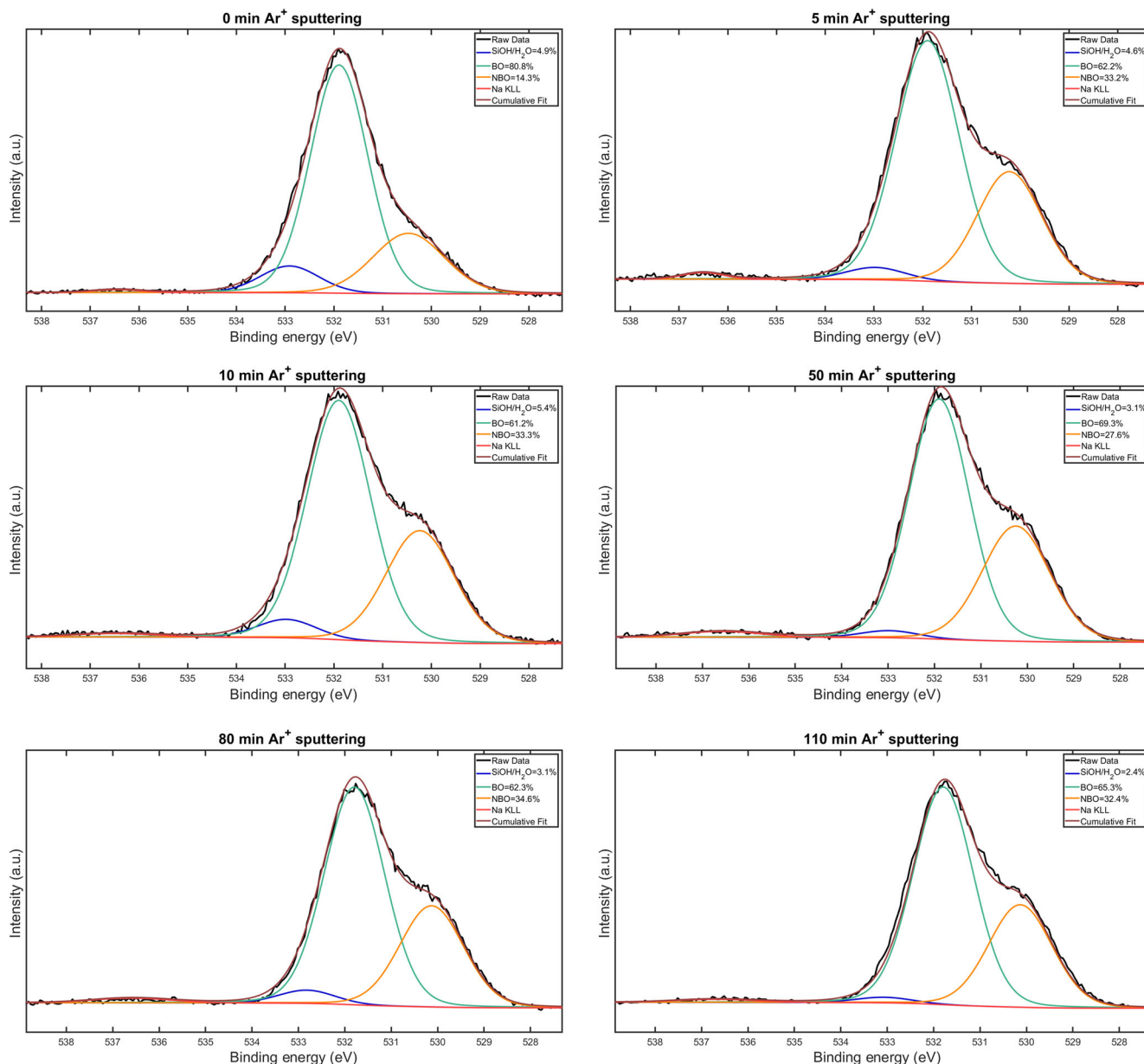


FIGURE 3 Gaussian-Lorentzian curve-fits of O1s spectral lines—illustrating the variation of bridging oxygen (BO), non-bridging oxygen (NBO), and SiOH/H₂O species as a function of Ar⁺ sputtering time: (i) 0 min (surface measurement without sputtering), (ii) 5 min, (iii) 10 min, (iv) 50 min, (v) 80 min, and (vi) 110 min. Inset-legends indicate the corresponding normalized integrated peak areas expressed in percentage.

it is highly likely that there are fewer electrons at the oxygen atom in Si-OH than Si-O-Si and Si-ONa. Thus, the electron-electron repulsion at the oxygen atom in Si-OH decreases, which leads to increased BE. This justifies the assignment of the 532-eV peak to SiOH/H₂O species. Similarly, sodium, bearing the lowest electronegativity among the three elements, is accountable for a higher repulsion of the electron cloud at the oxygen atom in Si-ONa, consequently facilitating the ejection of O1s photoelectrons with a lower BE, in agreement with the proposition of Simonsen et al.²¹ This, in turn, justifies the assignment

of the intermediate peak at 531 eV to the Si-O-Si BO, owing to the intermediate position of silicon in the order of electronegativity of the three elements apart from oxygen, which undoubtedly possesses the highest electronegativity among the four elements in contention.

The integration of the peak areas gives an estimation of the concentration of the corresponding species. The concentration of each of the aforementioned species in the glass network was calculated with sequential XPS measurements accompanied by Ar⁺ sputtering (0–110 min of sequential sputtering at specific time intervals). A period of

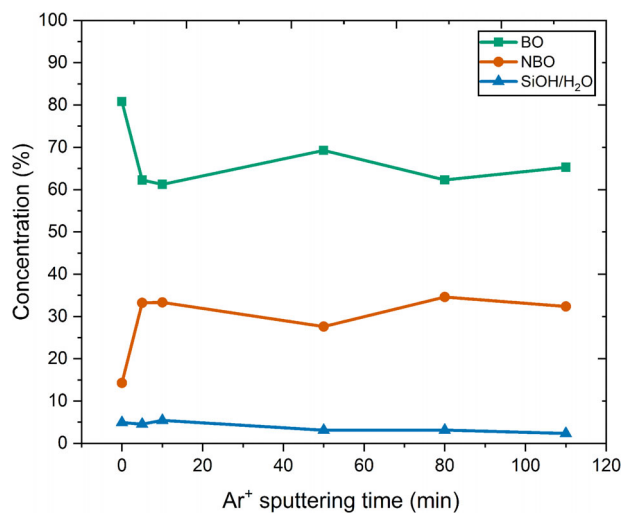


FIGURE 4 Quantitative illustration of variation of concentration (%) of bridging oxygen (BO), non-bridging oxygen (NBO), and SiOH/H₂O species with Ar⁺ sputtering time—calculated from the normalized integrated peak areas under the curve-fitted O1s spectra of Figure 2, reported in Table 1. Connecting lines act as guideline to the eyes.

110-min sputtering is estimated to be equivalent to a depth of ~110 nm of etching from the surface, considering an etching rate of around 1 nm/min according to a previous report on SLS glass (50 nm/h at 4 kV).²² The sputtering rate stated earlier is a fair assumption for an estimation of the overall probing depth of the thin subsurface layer considered in this study. The rate may not be constant throughout the sputtering duration due to the heterogeneity of the surface structure. It only gives an impression of the depth of interest for which the structural analysis has been elucidated in this paper. The respective O1s curve-fittings corresponding to sputtering times of 0 (surface measurement without sputtering), 5, 10, 50, 80, and 110 min are shown in Figure 3(i)–(vi). The variation of the NBOs, BOs, and SiOH/H₂O species with sputtering time, calculated from the corresponding normalized integrated peak areas of the curves presented in Figure 3, is illustrated in Figure 4.

It is to be noted that the data point corresponding to 0 min in Figure 4 corresponds to a measurement right on top of the glass surface without any sputtering. The information at this point in time is considered to be confined within a depth of 5 nm. The majority of the photoelectron signals were highly likely from the top 1- to 3-nm region. Theoretically, the information probing depth depends on the inelastic mean free path of the electrons, and the intensity of the signal decays exponentially with depth in the absence of elastic scattering of the photoelectrons.²⁰

The concentration of BO is higher than NBO throughout the entire depth of the sputtering range. Especially, the high ratio of BO to NBO on the surface up to a depth corresponding to 10 min of sputtering is to be emphasized. Furthermore, Figure 4 shows that the concentration of the SiOH/H₂O species is close to 5% right on the surface with a slightly decreasing trend with increasing depth. The silanol groups may be present in different forms, such as isolated silanols, vicinal silanols, geminal silanols, and hydrogen-bonded silanols,^{23–25} which compensate the depletion of sodium ions up to a shallow depth on the order of few nanometers from the surface. A sodium-depleted outer skin of SLS surface (first data point of Na1s in Figure 2) was reported by several studies, which is a common observation owing to its susceptibility to the volatilization of the outer glass skin.^{4,26} The outer glass skin is in incessant interaction with the ambient atmosphere that leads to the adsorption of chemisorbed and physisorbed water molecules to the silanol groups.

3.2 | Si2p curve-fittings

According to theory (Section 2), the Si2p curve should consist of two peaks, namely, a spin doublet—Si2p_{3/2} and Si2p_{1/2}, separated by .617 eV with equal FWHM, the ratio of magnitude of intensity of the peaks being Si2p_{3/2}:Si2p_{1/2} = 2. Figure 5 shows the Si2p spectral peak-fits (with corresponding BEs mentioned in legends), with respect to Ar⁺ sputtering time. In general, a chemical shift toward a higher BE of the Si2p signal is thought to qualitatively represent a dominant BO (Si–O–Si)-like behavior.^{10,26} However, the variation of the position of the BE of Si2p_{3/2} with sputtering time as experimentally obtained (see Table 2) was negligible, as it almost laid within the range of our best spectral resolution of .2 eV.

The corresponding areas under the curves, FWHM values, BE positions, and chi-squared values (goodness of fit) of the O1s and Si2p spectral fits with respect to sputtering time are tabulated in Table 2. The atomic ratio of O/Si was calculated by taking into consideration the corrected relative sensitivity factor (RSF) from the MultiPak database. The RSF is specific to the instrument used, as well as the element, and level the photoelectron emanated from—as it encompasses the parameters of photoelectron cross section, inelastic mean free path of the photoelectrons and instrument factors such as transmission function.¹⁸ The individual contributions of the three identified oxygen speciations and the total oxygen-to-silicon atomic ratios are reported in Table 3 and Figure 6.

Table 3 displays the total atomic ratio of oxygen to silicon (O_{total}/Si) throughout the depth associated with 110 min of Ar⁺ sputtering at specific time intervals, while separately

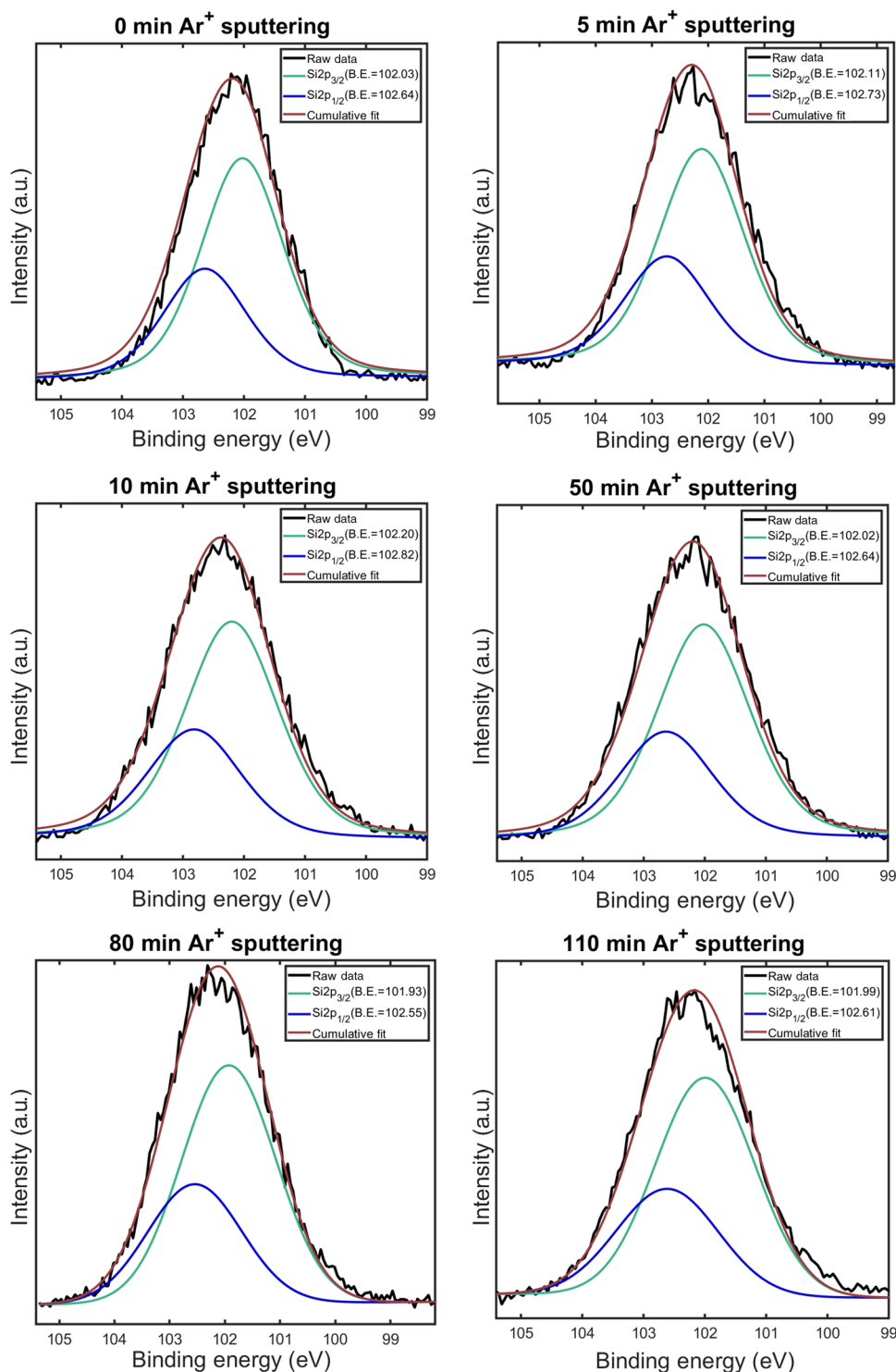


FIGURE 5 Curve-fitted Si2p spectral lines: Illustration of the chemical shift of binding energy (eV) with Ar⁺ sputtering time: (i) 0 min (without sputtering), (ii) 5 min, (iii) 10 min, (iv) 50 min, (v) 80 min, and (vi) 110 min

illustrating the contributions of individual components, namely, BOs ($O_{Si-O-Si}$), NBOs associated with sodium network modifier cations ($O_{Si-O-Na}$), and SiOH/H₂O species ($O_{SiOH/H_2O/Si}$). The atomic ratio of total oxygen content to silicon, O_{total}/Si (on the extreme right column), varied within the range of 2.94–3.74 throughout the depth of

sputtering range in decreasing order from the surface to the bulk, which was an interesting outcome. It is graphically portrayed in Figure 6. A high O/Si ratio is generally indicative of a depolymerized silicate network.²⁷ The presence of NBOs associated with network modifiers and hydrous species (SiOH/H₂O) in the subsurface network

TABLE 2 Percentage of area, binding energy (BE), full-width at half maxima (FWHM), and chi-squared (χ^2) values of O1s and Si2p spectral fits with Ar⁺ sputtering time

Sputtering time (min)	O1s						Si2p						
	BO (Si-O-Si)			NBO (Si-O-Na)			SiOH/H ₂ O			χ^2	Si2p _{3/2}		χ^2
	Area (%)	BE (eV)	FWHM (eV)	Area (%)	BE (eV)	FWHM (eV)	Area (%)	BE (eV)	FWHM (eV)		BE (eV)	FWHM (eV)	
0	80.8	531.75	1.58	14.3	530.03	1.36	4.9	532.74	1.30	2.02	102.03	1.60	6.63
5	62.2	531.80	1.45	33.2	530.13	1.56	4.6	532.71	1.50	3.60	102.11	1.80	4.95
10	61.2	531.90	1.45	33.3	530.25	1.56	5.4	532.71	1.50	3.60	102.20	1.80	3.50
50	69.3	531.73	1.58	27.6	530.01	1.36	3.1	532.74	1.30	3.70	102.02	1.80	2.88
80	62.3	531.74	1.45	34.6	530.08	1.56	3.1	532.71	1.50	4.41	101.93	2	1.49
110	65.3	531.80	1.54	32.4	530.12	1.56	2.4	532.71	1.50	2.49	101.99	1.90	2.24

Abbreviations: BO, bridging oxygen; NBO, non-bridging oxygen.

TABLE 3 Variation of oxygen to silicon atomic ratios (O/Si) calculated over Ar⁺ sputtering time, while taking into account the corrected relative sensitivity factor (RSF)

Sputtering time (min)	O _{Si-O-Si} /Si	O _{Si-O-Na} /Si	O _{SiOH/H₂O} /Si	O _{total} /Si
0	2.3	.78	.66	3.74
5	1.67	1.35	.21	3.23
10	1.61	1.2	.18	2.99
50	1.54	1.18	.32	3.05
80	1.57	1	.33	2.9
110	1.57	1.28	.09	2.94

of SLS glass increases the atomic ratio of O_{total}/Si from the otherwise known value of 2.0 for fused silica (SiO₂) consisting of all Q⁴ entities (four BOs without any NBO per silica tetrahedron). The experimental data point corresponding to 0 min of sputtering associated with the top surface consisted of the highest O_{total}/Si ratio of 3.74, which was theoretically logical, owing to the high abundance of silanol groups and associated hydrogen-bonded water molecules on the surface.^{27–29} However, the concentration of BO was experimentally found to be the highest at this point in depth. This unexpected outcome was confirmed to be true for the second category of SLS glass that was investigated separately, represented in Figure S3. This is proposed to be caused by repolymerization on the top surface due to the migration of sodium ions (during and after glass production and during argon ion sputtering), in accordance with the observation of Brow.³⁰ Thus, a high atomic ratio of O_{total}/Si does not necessarily represent a weak network connectivity, signified by the high contribution of O_{Si-O-Si}/Si at this point. The experimental evidence of the relatively high ratio of O_{SiOH/H₂O}/Si observed up to 10 min of sputtering validates the essence of association of NBOs with different forms of silanol groups on the surface

rather than sodium ions that were leached out of this thin layer (of about 10 nm or higher) due to its high mobility. The O_{total}/Si ratio showed a steady decreasing trend in the range of 0–10 min of sputtering (3.74–2.99, to be precise). Thereafter, with an increasing depth of sputtering, the ratio seemed to saturate in the range of 2.9–3, which theoretically corresponds to the Q² structure³¹ (two BOs and two NBOs linked to a silica tetrahedron). A similar trend was observed for the SLS glass slides analyzed additionally, with a saturation of O_{total}/Si around 3.2, as shown in Figure S3. This trend of saturation of the ratio close to 3 was also observed in our previous study.³² A stoichiometric ratio of 3.5 is theoretically representative of Q¹ structure associated with pyrosilicates (Si₂O₇)⁶⁻, marked by the presence of three NBOs linked to a silica tetrahedron. The experimental evidence proposes that the region constrained within a depth of about 1–3 nm (corresponding to the first data point without sputtering) is likely to be composed of Q⁰ (self-sustaining species) and Q¹ units—indicative of mechanically weakening structural entities. However, this does not completely rule out the likelihood of the presence of stronger Qⁿ units (*n*: 2–4), considering the contribution of O_{Si-O-Si}/Si, although the probability

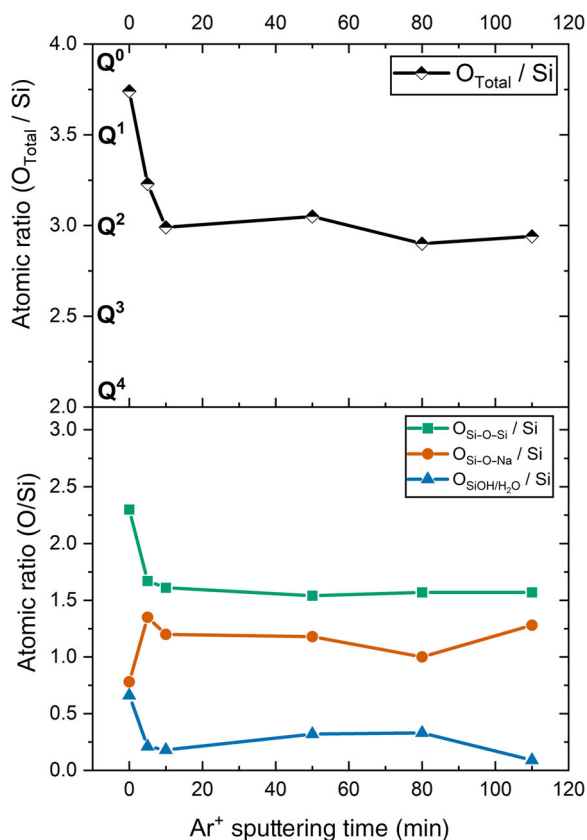


FIGURE 6 Variation of the atomic ratio of individual oxygen speciations to silicon, as a function of Ar⁺ sputtering time (below); variation of atomic ratio of total oxygen (sum of individual contributions) to silicon, as a function of Ar⁺ sputtering time (above). Connecting lines act as guideline to the eyes.

of encountering Q³ and Q⁴ species at this depth is lower compared to the bulk. The Qⁿ species marked alongside the experimentally obtained atomic ratio of O_{total}/Si in Figure 6 gives an overall insight of the subsurface silicate network connectivity from theoretical perspective. In this case, the drawback associated with sole reliance on XPS analysis was quite evident in terms of its inability to quantifiably determine separate Qⁿ species in the overall glass network apart from the near-surface region—in accordance with the observation of Nesbitt et al.¹⁰

The contribution of the individual network modifier cations to the total concentration of NBOs may be stoichiometrically calculated, along with the concentrations of BOs and SiOH/H₂O, by the following system of equations, considering charge neutrality and mass balance⁸:

$$\begin{aligned} \text{NBO} &= 2[\text{Ca}] + 2[\text{Mg}] + [\text{Na}] - [\text{Al}] \\ [\text{OH} + \text{H}_2\text{O}] &= |(-2) \times [\text{O}_{\text{total}}] + (1 \times [\text{Na}] + 2 \times [\text{Ca}] + 2 \times [\text{Mg}] + 3 \times [\text{Al}] + 4 \times [\text{Si}])| \\ \text{BO} &= [\text{O}_{\text{total}}] - [\text{NBO}] - [\text{OH} + \text{H}_2\text{O}] \end{aligned}$$

This paper adopted the approach of O1s peak-fitting to separately determine the contributions of BOs, NBOs, and SiOH/H₂O, as a function of depth from the glass surface by Ar⁺ sputtering. This was done to avoid the drawbacks associated with Ar⁺ sputtering in causing the migration of mobile modifier cations to affect their respective concentrations. It would consequently affect the concentrations of the different oxygen speciations in the aforementioned system of equations with misleading results, when calculated as a function of depth from the glass surface.

The depth of the glass surface from which the photoelectrons are ejected as a consequence of bombardment of X-rays during the XPS measurements depends on their kinetic energy, which in turn is dependent on the BE of the electrons. The difference in BE between Si2p and O1s is just over 400 eV, which is quite high. Hence, it may so happen that the photoelectrons emitted from O1s and Si2p orbitals used for analysis in this paper may have been ejected from slightly different depths below the glass surface corresponding to a particular cycle of sputtering (the difference probably being in the range of a couple of nanometers or even less) due to their differences in BEs. This was one of the major reasons behind the exclusion of Na1s from our calculations, owing to its BE being close to 1075 eV (the massive gradient of BEs between Na1s and O1s, as well as Na1s and Si2p shall not be neglected to avoid erroneous interpretation), although sodium is thought to play a vital role in terms of its association with NBOs except on the outer surface owing to its high susceptibility to volatilization—ensuing our preceding discussion. The prolonged exposure of the glass surface to X-rays (>10 h) accompanied by low-energy electrons to compensate surface charge buildup is reportedly known to have a pronounced effect to decrease the atomic ratio of O_{total}/Si, as a consequence of oxygen depletion caused by outgassing of free oxygen to the surrounding vacuum released by the breakage of NBO bonds.³² The concentration of NBO increases with decrease in BO concentration with time. However, the duration of XPS experiments accompanied by Ar⁺ sputtering reported in this study is significantly shorter to repudiate the possibility of detrimental surface damage effects associated with the breakage of silicate network. The analysis of the network modifiers has been avoided due to the migration of mobile ions that is known to be caused by Ar⁺ sputtering.³³ Consequently, the

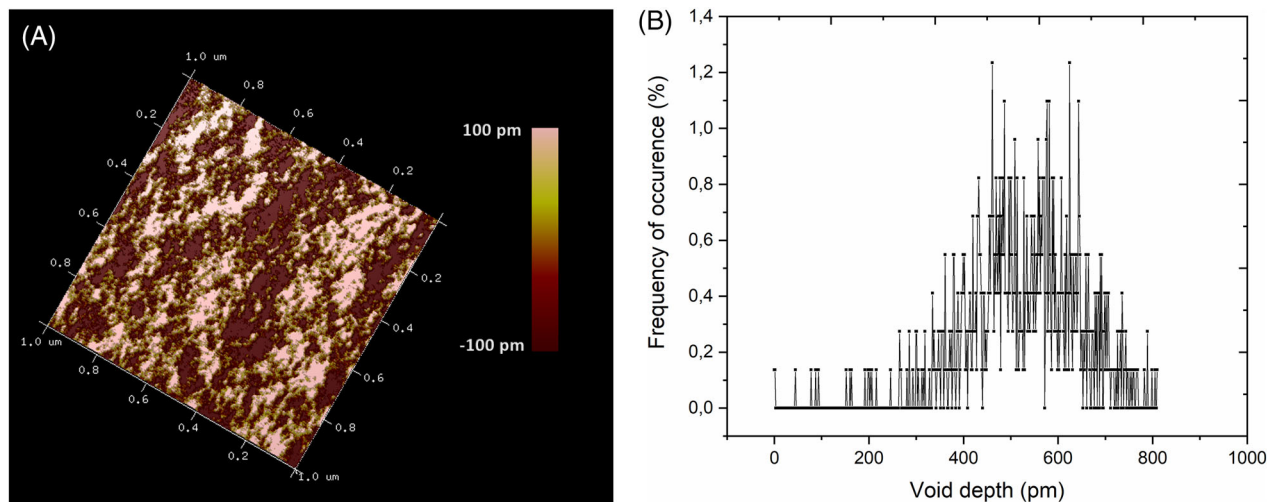


FIGURE 7 (A) A $1 \times 1\text{-}\mu\text{m}^2$ atomic force microscopy (AFM) representation of the top surface with z-resolution ~ 100 pm—pink: surface silicate network; brown: distribution of intertetrahedral voids within the silicate network marked by the presence of nano-channelized pathway and (B) depth-histogram of the inherent voids between top two monolayers

structural analysis reported in this paper has been solely confined to O1s and Si2p spectral lines, to determine the silicate network connectivity of the near-surface region of SLS glass.

According to Zachariasen's classical rules of glass formation,³⁴ no oxygen atom may be linked to more than two cations. Thus, each BO must be linked to two silicon atoms in the studied SLS glass. A BO, in general, is also linked to the intermediate element, Al, to form Si–O–Al network for glasses with high alumina content, for example, calcium aluminosilicate glass. The negligible presence of aluminum in the SLS glass surface considered in this study (evidenced by the absence of any pronounced detectable Al2p peak in the XPS survey spectrum shown in Figure 1) eliminated the necessity of its mention elsewhere in the paper. It is to be noted that a high $O_{\text{total}}/\text{Si}$ ratio does not necessarily indicate silicate network depolymerization, considering the possible presence of interstitial water molecules within the network that could increase the contribution of $O_{\text{SiOH}/\text{H}_2\text{O}}$. However, the authors consider the glass surface to be constituted of a mechanically weakened network,³¹ specifically attributed to the high contribution of SiOH/ H_2O species with a high likelihood of the maximum contribution from silanol groups associated with NBOs. This is characteristic of a vulnerable surface structure. Any injury to the glass skin provides pathways for interaction with the surrounding media and gives rise to propagation of surface-initiated cracks or diffusion processes.⁴ The vulnerability of the surface is expressed by the distribution of voids on the top surface, which were investigated by atomic force microscopy. Figure 7A shows the AFM representation of the prepared

top surface layer, mapped by silicate islands (pink, light color) surrounded by pits and voids (brown, dark color). The distribution of the depths of voids at the top surface, which correspond to approximately two silicate layers, is represented by the histogram in Figure 7B. The frequency of occurrence of the void-depths (obtained by scanning three different spots of $1\ \mu\text{m}^2$ on the top surface) is constrained within the range of 450–650 pm—potentially a representative of the availability of a directional pathway for propagation of a crack front through the depth of the glass network.³⁵ Overall, a weak surface network connectivity owing to the adsorption of hydrous species (SiOH/ H_2O), disseminated by intertetrahedral voids, constitutes the structural weakness of the surface network of SLS glass.

4 | CONCLUSION

This study predominantly explored the structural chemistry of SLS glass surface as a function of depth by means of sequential XPS measurements, accompanied by Ar^+ sputtering. The concentrations of BOs, NBOs, and hydrous species (SiOH/ H_2O) were separately calculated by O1s spectral fits with sputtering time of up to 110 min. The concentration of BO was found to be consistently higher than NBO throughout the depth of sputtering of about 100 nm. The concentration of SiOH/ H_2O species was less than 10% throughout the scanned depth, with its apex being confined to the top surface up to about 10 nm, owing to the inevitable interaction of the glass surface with ambient atmosphere.

The curve-fittings of Si₂p doublet did not yield any suitably specific contribution with respect to any noticeably significant shift in BE of Si₂p_{3/2}. The atomic ratio of oxygen to silicon (O/Si) was calculated by taking into consideration the corrected RSF. The individual contributions of BOs (O_{Si-O-Si}/Si), NBOs (O_{Si-O-Na}/Si), and SiOH/H₂O species (O_{SiOH/H₂O}/Si) were calculated to formulate the atomic ratio of O_{total}/Si as a function of depth from the glass surface, which is characteristic of the variation of coordination number of silicon associated with Qⁿ species (where *n* represents the number of BOs linked to a silica tetrahedron). A high O_{total}/Si atomic ratio does not necessarily indicate network depolymerization, considering the contribution of interstitial water molecules within the network that could also increase the O_{total}/Si ratio. It was found that the surface up to a depth of about 1–3 nm had the maximum O_{total}/Si ratio of 3.74, with a decreasing trend close to 3.0 (Q² species) up to an Ar⁺ sputtering time of 10 min followed by tending to attaining a saturation up to 110 min of sputtering. This was indeed an interesting experimental finding with respect to proving the surface-weakening effect predominantly caused by the silanol groups associated with Q⁰ and Q¹ species—accountable for providing a nano-channelized pathway for a surface-initiated crack front to propagate through the inherent intertetrahedral voids of depths in the range of 450–650 pm, acting as a probable indicator for the vulnerability of the surface and an initial point for brittle fracture.

ACKNOWLEDGMENTS

We gratefully acknowledge the financial support within the ForCycle II program of “Bavarian State Ministry of the Environment and Consumer Protection,” under Grant number BAF0150Fo-74094. The access to the XPS/UPS facility (PHI 5000 VersaProbe III system) at the Device Engineering KeyLab in the Bavarian Polymer Institute, University of Bayreuth is gratefully acknowledged. The access to the AFM Keylab in the chair of Physical Chemistry II, University of Bayreuth is acknowledged.

Open access funding enabled and organized by Projekt DEAL.

AUTHOR CONTRIBUTION

Barsheek Roy: Conceptualization, methodology, analysis, writing—original draft

Felix Baier: Experimentation, data curation

Andreas Rosin: Writing—review and editing, validation


Thorsten Gerdes: Validation, approval

Stefan Schafföner: Writing—review and editing, final approval.

ORCID

Barsheek Roy  <https://orcid.org/0000-0003-4876-2023>

Andreas Rosin  <https://orcid.org/0000-0001-8835-5057>

Stefan Schafföner  <https://orcid.org/0000-0002-6526-2496>

REFERENCES

- Ziemath EC. Degradation of the surface of a meta silicate glass due to atmospheric moisture. *Quim Nova*. 1998;21(3):356–60.
- Papadopoulos N, Drosou CA. Influence of weather conditions on glass properties. *J Univ Chem Technol Metall*. 2012;47:429–38.
- Majerus O, Lehuède P, Biron I, Alloteau I, Narayanasamy S, Caurant D. Glass alteration in atmospheric conditions: crossing perspectives from cultural heritage, glass industry, and nuclear waste management. *NPJ Mater Degrad*. 2020;4(1):27–42.
- Wang C, Häfner W, Krausch G, Rädlein E, Tratzky S, Schramm M, et al. Study of surface changes on industrial glasses with AFM, FE-SEM, EDX, SNMS and LM Part 1. Glass skin and corrosion. *Glass Sci Technol*. 2004;77:103–10.
- Clark DE, Dilmore MF, Ethridge EC, Hench LL. Aqueous solution of soda-silica and soda-lime-silica glass. *J Am Ceram Soc*. 1976;59:62–5.
- Hellmann R, Cotte S, Cadel E, Malladi S, Karlsson LS, Lozano-Perez S, et al. Nanometre-scale evidence for interfacial dissolution-precipitation control of silicate glass corrosion. *Nat Mater*. 2015;14(3):307–11.
- Sheth N, Luo J, Banerjee J, Pantano CG, Kim SH. Characterization of surface structures of dealcalized soda lime silica glass using X-Ray photoelectron, specular reflection infrared, attenuated total reflection infrared and sum frequency generation spectroscopies. *J Non-Cryst Solids*. 2017;474:24–31.
- Banerjee J, Bojan V, Pantano CG, Kim SH. Effect of heat treatment on the surface chemical structure of glass: oxygen speciation from in situ XPS analysis. *J Am Ceram Soc*. 2017;101(2):644–56.
- Sprenger D, Bach H, Meisel W, Gütlich P. XPS study of leached glass surfaces. *J Non-Cryst Solids*. 1990;126:111–29.
- Nesbitt HW, Bancroft GM, Henderson GS, Ho R, Dalby KN, Huang Y, et al. Bridging, non-bridging and free (O²⁻) oxygen in Na₂O-SiO₂ glasses: an X-ray photoelectron spectroscopic (XPS) and nuclear magnetic resonance (NMR) study. *J Non-Cryst Solids*. 2011;357(1):170–80.
- Reiß S, Urban S, Jacob K, Krischok S, Rädlein E. Investigation of the influence of a commercial glass protector on float glass surfaces by x-ray photoelectron spectroscopy. *Phys Chem Glasses: Eur J Glass Sci Technol, B*. 2017;58:99–108.
- Pantano CG, Kelso JF, Suscavage MJ. Surface studies of multicomponent silicate glasses: quantitative analysis, sputtering effects and the atomic arrangement. In: Rossington DR, Condrate RA, Snyder R. *Advances in materials characterization*. vol. 15., Boston, MA: Springer; 1983
- Zemek J, Jiricek P, Houdkova J, Jurek K, Gedeon O. Lead-silicate glass surface sputtered by an argon cluster ion beam investigated by XPS. *J Non-Cryst Solids*. 2017;469:1–6.

14. Yamamoto Y, Yamamoto K. Ar ion damage on the surface of soda-lime-silica glass. *IOP Conf Ser: Mater Sci Eng.* 2011;18(2):022005.
15. Yamamoto Y. Precise XPS depth analysis of soda-lime-silica glass surface after various treatments. *Surf Interface Anal.* 2012;44(8):931–3.
16. Yamamoto Y, Yamamoto K. Precise XPS depth profile of soda-lime-silica float glass using C60 ion beam. *Opt Mater.* 2011;33(12):1927–30.
17. Shirley DA. High-resolution X-ray photoemission spectrum of the valence bands of gold. *Phys Rev B.* 1972;5:4709–14.
18. van der Heide P. X-ray photoelectron spectroscopy: an introduction to principles and practices. Hoboken: John Wiley & Sons, Inc.; 2012.
19. Pleul D, Frenzel R, Eschner M, Simon F. X-ray photoelectron spectroscopy for detection of the different Si-O bonding states of silicon. *Anal Bioanal Chem.* 2003;375:1276–81.
20. Greczynski G, Hultman L. X-ray photoelectron spectroscopy: towards reliable binding energy reference. *Prog Mater Sci.* 2020;107:100591.
21. Simonsen ME, Sønderby C, Li Z, Sogaard EG. XPS and FT-IR investigations of silicate polymers. *J Mater Sci.* 2009;44:2079–88.
22. Yamanaka H, Yamashita M, Matsuoka J, Wakabayashi H, Terai R. Depth profiling by XPS for corroded glass. *J Non-Cryst Solids.* 1990;116:286–8.
23. Garofalini SH. Simulations of glass surfaces: structure and adsorption. Dordrecht: Springer Netherlands; 1994. p. 375–90.
24. Christy AA. The nature of silanol groups on the surfaces of silica, modified silica and some silica based materials. *AMR.* 2014;998–999:3–10.
25. Dunker HH. Glass surfaces. Amsterdam: Elsevier; 1982. p. 1–74.
26. Mekki A, Holland D, McConville CF, Salim M. An XPS study of iron sodium silicate glass surfaces. *J Non-Cryst Solids.* 1996;208:267–76.
27. Santhy K, Sowmya T, Sankaranarayanan SR. Effect of oxygen to silicon ratio on the viscosity of metallurgical slags. *ISIJ Int.* 2005;45:1014–8.
28. Lin YT, Smith NJ, Banerjee J, Agnello G, Manley RG, Walczak WJ, et al. Water adsorption on silica and calcium-boroaluminosilicate glass surfaces—thickness and hydrogen bonding of water layer. *J Am Ceram Soc.* 2020;104:1568–80.
29. Ngo D, Liu H, Chen Z, Kaya H, Zimudzi TJ, Gin S, et al. Hydrogen bonding interactions of H₂O and SiOH on a boroaluminosilicate glass corroded in aqueous solution. *NPJ Mater Degrad.* 2020;4:1.
30. Brow RK. Glass surface modifications during ion beam sputtering. *J Non-Cryst Solids.* 1988;107:1–10.
31. Shelby JE. Introduction to glass science and technology. 3rd ed. London: The Royal Society of Chemistry; 2021.
32. Roy B, Rosin A, Gerdes T, Schafföner S. Revealing the surface structural cause of scratch formation on soda-lime-silica glass. *Sci Rep.* 2022;12:1–13. 2681.
33. Sharma A, Jain H, Miller AC. Surface modification of a silicate glass during XPS experiments. *Surf Interface Anal.* 2001;31:369–74.
34. Zachariasen WH. The atomic arrangement in glass. *J Am Chem Soc.* 1932;54(10):3841–51.
35. Wondraczek L, Mauro JC, Eckert J, Kühn U, Horbach J, Deubener J, et al. Towards ultrastrong glasses. *Adv Mater.* 2011;23:4578–86.

SUPPORTING INFORMATION

Additional supporting information can be found online in the Supporting Information section at the end of this article.

How to cite this article: Roy B, Baier F, Rosin A, Gerdes T, Schafföner S. Structural characterization of the near-surface region of soda–lime–silica glass by X-ray photoelectron spectroscopy. *Int J Appl Glass Sci.* 2023;14:229–239.
<https://doi.org/10.1111/ijag.16604>